



Performance-Based Seismic Design of Nonstructural Building Elements

Andre Filiatrault, Daniele Perrone, Roberto Javier Merino & Gian Michele Calvi

To cite this article: Andre Filiatrault, Daniele Perrone, Roberto Javier Merino & Gian Michele Calvi (2018): Performance-Based Seismic Design of Nonstructural Building Elements, Journal of Earthquake Engineering, DOI: [10.1080/13632469.2018.1512910](https://doi.org/10.1080/13632469.2018.1512910)

To link to this article: <https://doi.org/10.1080/13632469.2018.1512910>



Published online: 14 Sep 2018.



Submit your article to this journal [↗](#)



Article views: 401



View related articles [↗](#)



View Crossmark data [↗](#)



Performance-Based Seismic Design of Nonstructural Building Elements

Andre Filiatrault^{a,b}, Daniele Perrone^a, Roberto Javier Merino^a, and Gian Michele Calvi^a

^aUniversity School for Advanced Studies IUSS Pavia, Pavia, Italy; ^bDepartment of Civil, Structural and Environmental Engineering, the State University of New York at Buffalo, Buffalo, NY, USA

ABSTRACT

Performance-based earthquake engineering requires the harmonization of performances between structural and nonstructural elements. This paper discusses the performance-based seismic design of nonstructural elements through a direct displacement-based methodology applicable to nonstructural elements attached to a single location in the supporting structure and for which damage is the result of excessive displacements. The fundamentals of direct displacement-based seismic design are presented along with a description of the modifications required for its application to nonstructural elements. As an example, the direct displacement-based seismic design of a suspended piping restraint installation is presented. The design approach is appraised by nonlinear dynamic time-history analyses.

ARTICLE HISTORY

Received 9 April 2018
Accepted 14 August 2018

KEYWORDS

Direct Displacement-Based Seismic Design; Earthquakes; Nonstructural Elements; Nonstructural Components; Pipes; Suspended Piping Restraint Installations

1. Introduction

A seminal advancement in earthquake engineering over the last two decades has been the elaboration of performance-based concepts for the seismic design of structures. Although this approach, based on the coupling of multiple performance limit states and seismic hazard levels, has advanced substantially for some types of structural systems to the point where it is starting to be incorporated into building codes and standards [e.g., ASCE, 2017], its application to nonstructural building elements remains largely unexplored.

Nonstructural elements and systems are not part of a building's structural load-bearing system but are nonetheless subjected to the same dynamic environment during an earthquake. In many earthquakes that have struck densely built regions in the twentieth century [Filiatrault *et al.*, 2001; Chock *et al.*, 2006; Gupta and McDonald, 2008; Ricci *et al.*, 2011; Salvatore *et al.*, 2009; Ercolino *et al.*, 2012; Perrone *et al.*, 2018], nonstructural losses have exceeded structural losses in most affected buildings. This is not surprising considering that nonstructural elements account for most of the investment in a typical building [Miranda and Taghavi, 2003] and that nonstructural elements typically incorporate primitive seismic design based on prescriptive empirical regulations and guidelines [Filiatrault and Sullivan, 2014].

In comparison to structural elements and systems, there is much less information and specific guidance available on the seismic design of nonstructural building elements for

multiple-performance levels. There has not been much basic research in this area and design engineers are often forced to start almost from scratch: observe what went wrong and try to prevent it from happening again. This is a consequence of the prescriptive design information currently available being based for the most part on judgment and intuition rather than on scientific experimental and analytical results. Summaries of many important aspects of the seismic behavior of nonstructural building elements as well as the evolution of research and code efforts in the last 30 years can be found in Soong [1995] and Filiatrault and Christopoulos [2002].

For seismic damage assessment purposes, nonstructural elements are often classified into two categories: “acceleration-sensitive” or “displacement-sensitive” nonstructural elements [FEMA, 2012]. Damage to acceleration-sensitive nonstructural elements is mainly caused by inertia forces arising from horizontal and/or vertical accelerations at various levels in the supporting structure, causing overturning or excessive sliding/displacement of the elements. Examples of acceleration-sensitive nonstructural elements are suspended building utility systems, such as piping systems and cable trays, and anchored or free standing building utility systems or contents. Damage to displacement-sensitive nonstructural elements is mainly caused by inter-story displacements or drifts in the supporting structure, causing excessive distortions in the elements. Examples of displacement-sensitive nonstructural elements are architectural elements, such as windows, partitions, and other items that are tightly attached into the supporting structure. Most code-based seismic design provisions implicitly consider both acceleration-sensitive elements, by specifying equivalent static design forces, and displacement-sensitive elements, by imposing drift limits on the supporting structure or relative displacements limit between the elements and the supporting structure. Because of lack of information, current seismic design provisions are empirical in nature and lack clear definitions of performance objectives under specific seismic hazard levels.

Nonstructural building elements would benefit greatly from rational performance-based seismic design procedures. Focusing on acceleration-sensitive nonstructural elements, it can be argued that these elements behave similarly to structural systems except for their different dynamic characteristics and the seismic input motions coming from the floors in the supporting structure at which they are attached rather than from ground motions. Furthermore, the labeling of “acceleration-sensitive” nonstructural elements is somewhat fallacious since, in the end, damage in many of these elements results from excessive relative displacements from the supporting structure that they are attached to. With this in mind, this paper elaborates a performance-based seismic design procedure for acceleration-sensitive nonstructural building elements using a direct displacement-based methodology. The proposed design procedure applies mainly to acceleration-sensitive nonstructural elements suspended or anchored at a single location (floor) of the supporting structure and for which damage is the result of excessive displacements. Nonstructural typologies for which the proposed direct displacement-based seismic design procedure applies include piping systems (including sprinklers), cable trays, suspended ceilings, cantilevered parapets, raised access floors, anchored shelves and out-of-plane partitions, cladding, and glazing.

2. Current Force-Based Seismic Design of Nonstructural Building Elements

The primary intent of current seismic design requirements for nonstructural building elements in North America and Europe [ASCE, 2016; NRC, 2015; CEN, 2004] is to

maintain life-safety. This is attempted by limiting large displacements of nonstructural elements by anchoring them to the supporting structure and by minimizing the potential for internal damage to nonstructural elements, particularly in critical facilities. Current seismic design requirements are based on the fundamental assumption that nonstructural elements can be considered dynamically uncoupled from the structural system to which they are connected, thereby justifying a “cascading” design approach. In this approach, the dynamic floor responses of the supporting structure are estimated first, without considering the interaction with the nonstructural elements. The structural response at the attachment level is then considered as input for the estimation of the response of the nonstructural elements.

In current North American and European design standards, the seismic design of nonstructural elements starts by the calculations of equivalent static design forces in the horizontal and/or vertical directions, and applying these forces to the element’s center of mass. The equivalent static design forces are calculated by multiplying the mass of the nonstructural element by the corresponding peak horizontal and/or vertical accelerations anticipated at its center of mass during the design seismic event. Similar to building structures, the equivalent static forces for the design of essential (critical) nonstructural elements are multiplied by an importance factor larger than unity. In addition, to account for the overstrength and nonlinear response of nonstructural elements, the equivalent static design forces are divided by a response modification factor larger than unity. The support reactions due to the equivalent static design forces are usually calculated based on the mass distribution of the nonstructural element [Meisel, 2001; Tauby *et al.*, 1999]. Finally, the connections and restraints must be designed to withstand these equivalent static forces. For nonstructural elements required for life-safety or continuous operation of important facilities, the elements themselves must be designed also for these same equivalent static forces.

In the Eurocode 8, for example, the horizontal equivalent static design force, F_a , to be applied at the center of mass in the most unfavorable direction of a nonstructural element can be obtained from CEN [2004]:

$$F_a = \frac{S_a \gamma_a}{q_a} W_a \quad (1)$$

In Eq. [1], W_a is the operating weight of the element, γ_a is the importance factor (equal to 1.0 for a normal importance element and 1.5 for an element required for life-safety or containing hazardous materials), q_a is the behavior (force reduction) factor taking the value of 1.0 or 2.0 depending on the types of nonstructural elements [CEN, 2004]. S_a in Eq. [1] is the seismic coefficient (design acceleration normalized by the acceleration due to gravity) that may be calculated from the following expression:

$$S_a = a_g S \left(\frac{3(1 + z/H)}{1 + (1 - T_a/T_n)^2} - 0.5 \right) \geq a_g S \quad (2)$$

where a_g is the peak ground acceleration (in units of g) for a rock site for the design earthquake the intensity of which each country in Europe specifies within their own national annex, but which typically corresponds to an event with a return period of 475 years. S in Eq. [2] is a soil factor (1.0 for rock sites and generally larger for softer soil sites), H is the

total height of the supporting structure, and z is the elevation of the nonstructural element measured from above the foundation level. T_a in Eq. [2] is the elastic vibration period of the nonstructural element and T_n is the elastic fundamental (first-mode) vibration period of the supporting structure in the relevant direction of excitation.

Although the simple forced-based design approach for nonstructural elements has been used extensively since its introduction in the 1964 edition of the Uniform Building Code [UBC, 1964] in the United States and remains the cornerstone of seismic design requirements included in current editions of design codes, it includes several major shortcomings. These shortcomings, expressed both in general terms and more specifically in terms of the Eurocode 8 force-based design procedure, are itemized below.

- (1) The force-based design process is initiated with estimates of the elastic fundamental periods of the supporting structure and of the nonstructural element (T_n and T_a , respectively, in Eq. [2]). The estimation of the fundamental period of a nonstructural element is difficult to establish with all the uncertainties involved and with no specific guidelines in design codes. In fact, the whole notion of using structural and nonstructural elastic periods is fallacious since both the supporting structure and nonstructural elements are expected to exhibit inelastic seismic responses.
- (2) The empirical linear amplification of the peak floor acceleration with respect to the peak ground acceleration ($1 + z/H$ term in Eq. [2]) assumes first mode response of the supporting structure. The establishment of reasonable estimates for the peak floor acceleration response profile along the height of buildings has been the subject of numerous studies and is still controversial due particularly to higher mode effects in buildings [Singh *et al.*, 2006a, 2006b; Kehoe and Hachem, 2003; Miranda and Taghavi, 2003; Pekcan *et al.*, 2003; Drake and Bachman, 1996].
- (3) The component amplification factor [$3/(1 + (1 - T_a/T_n)^2$ term in Eq. [2]], representing the expected dynamic amplification of the peak floor acceleration at the center of mass of the nonstructural element, does not consider the damping characteristics of the element and neglects nonlinear response of both the supporting structure and of the nonstructural element.
- (4) The force reduction (behavior) factor assigned to the nonstructural element [q_a in Eq. [1]] is difficult to justify since it is based primarily on judgment. Particularly, the lack of information on the lateral load-deformation response of many nonstructural element typologies makes the use of current nonstructural force reduction factors misleading.
- (5) Deformation limit states of nonstructural elements are not directly addressed by the force-based design procedure. Limiting deformations is paramount for nonstructural elements, as stated qualitatively in building codes, since a large portion of the nonstructural damage from recent earthquakes has been associated with excessive lateral displacements.
- (6) The reduction of the equivalent elastic design force by a force reduction factor implies that the maximum displacement that the nonstructural element would undergo relative to the supporting structure if it would remain elastic is equal to the maximum displacement of the actual inelastic nonstructural element. This

equal displacement approximation is inappropriate for most short-period nonstructural element typologies.

- (7) Nonstructural force reduction factors are associated with the global displacement ductility capacity of the nonstructural element. This displacement ductility is based on the ratio of a performance limit displacement to a first-yield displacement. No appropriate definitions of yield and performance limit displacements have been formulated for nonstructural elements.

These limitations of the forced-based seismic design procedure do not allow for a proper assessment of the seismic safety of nonstructural building elements considering the various limit states that these elements may have to confront during their service lives. A performance-based seismic design approach for nonstructural elements should consider relative displacements to the supporting structure as the central focus of the design process. For many acceleration-sensitive nonstructural elements, this can be achieved by using a direct displacement-based seismic design procedure.

3. Fundamentals of Direct Displacement-Based Seismic Design of Supporting Structures

The central concept of the direct displacement-based seismic design method for supporting structures, as originally proposed by Priestley [1993, 1998, 2000] and since then elaborated in detail [Priestley *et al.*, 2007], is that the seismic design of the structure is based on a specified target displacement for a given seismic hazard level. For this purpose, the structure is modeled as an equivalent single-degree-of-freedom (SDOF) system with appropriate height and equivalent elastic lateral stiffness and viscous damping properties, representative of the global behavior of the actual structure at the target displacement. Figure 1 presents a flow chart illustrating the various steps of the direct displacement-based seismic design process for supporting structures. These various steps are briefly described below.

Step 1: Definition of Target Structural Displacement and Seismic Hazard

The first step in the design procedure is the definition of the target displacement, Δ_b , that the structural system should not exceed under a given seismic hazard level. Knowing Δ_t with an estimate of the yield displacement of the supporting structure, the target ductility ratio, μ_b , can be immediately derived. The seismic hazard associated with the target displacement must then be defined in terms of a design ground relative displacement response spectrum. For the life-safety limit state, corresponding to a return period of 475 years in most design codes, this can be easily obtained, for example, by transforming the 5% damped code design spectral accelerations for a given seismic zone, $S_{A5\%}$, into corresponding spectral displacement values, $S_{D5\%}$.

$$S_{D5\%} = \frac{T^2}{4\pi^2} S_{A5\%} \quad (3)$$

where T is the structural period.

Code design spectral values are typically specified for an equivalent viscous damping level equal to 5% of critical. Because inelastic structural response is expected under design

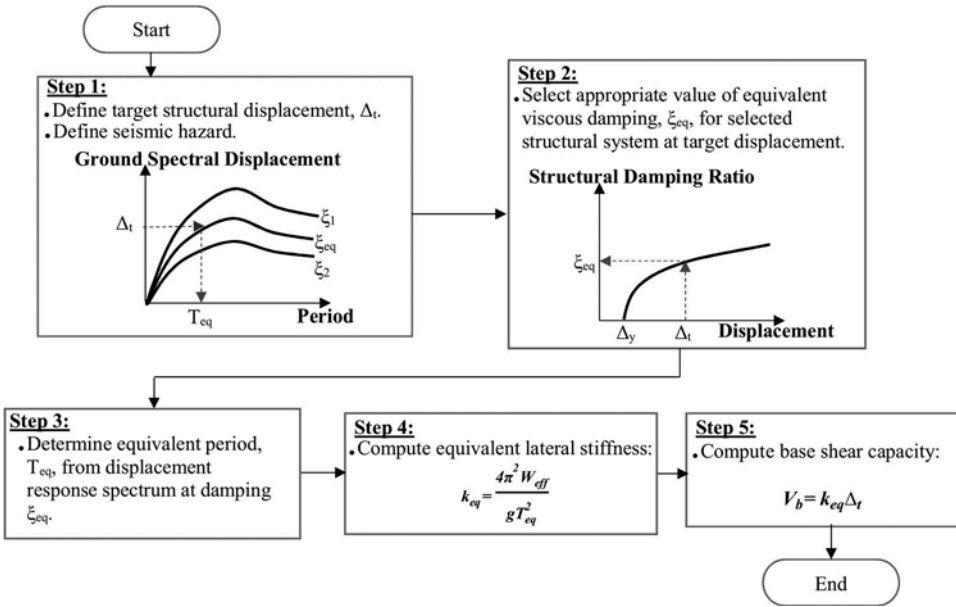


Figure 1. Flowchart of direct displacement-based seismic design of supporting structures.

ground motions, the resulting hysteretic energy dissipation can be represented by an equivalent viscous damping ratio in the structure higher than 5% of critical, as discussed in the next step. The spectral displacement values corresponding to the actual equivalent viscous damping level of the structure, $S_{D\xi_{eq}}$, can be obtained through empirical modification factors such as [CEN, 2004]:

$$S_{D\xi_{eq}} = S_{D5\%} \sqrt{\frac{0.10}{0.05 + \xi_{eq}}} \quad (4)$$

Note that if the design is to be conducted for a seismic hazard level different than the return period specified by the code (usually 475 years), the design displacement spectral values must be scaled based on the hazard curve for the site of the supporting structure.

Step 2: Determination of Structural Equivalent Viscous Damping

In order to capture the energy dissipation characteristics of the structure at the target displacement Δ_t , an equivalent viscous damping ratio, ξ_{eq} , must be determined. The equivalent viscous damping is generally estimated as a function of the ductility demand, which depends on the target displacement, defined in the previous step, and on the equivalent yield displacement, which can be estimated from simple equations [Priestley *et al.*, 2007]. To establish this damping database in the form of $\xi_{eq} - \Delta_t$ (or $\xi_{eq} - \mu_t$) relationship, the energy-based equivalent viscous damping approach originally proposed by Jacobsen [1930, 1960] is often used, as given by

$$\xi_{eq} = \frac{E_{D, \Delta_t}}{2\pi k_{eq} \Delta_t^2} + \xi_i \quad (5)$$

where E_{D,Δ_t} is the energy dissipated per cycle from the global hysteretic behavior of the structure at the target displacement, Δ_t , and k_{eq} is the equivalent (secant) lateral stiffness of the structure at the same target displacement. A nominal inherent damping ratio, ξ_i , is considered to account for the energy dissipation not associated with the hysteretic response of the structural system. Note that some of the inherent energy dissipation at small response amplitudes could result from interactions (e.g., friction) between non-structural elements and the supporting structure [Dwairi *et al.*, 2007].

Step 3: Determination of Structural Equivalent Period

Knowing the target displacement, Δ_t , and the equivalent viscous damping ratio, ξ_{eq} , of the structure at that target displacement, the equivalent period of the structure, T_{eq} , can be obtained directly from the design ground relative displacement response spectrum.

Step 4: Computation of Structural Equivalent Lateral Stiffness

Representing the supporting structure as an equivalent linear SDOF system, the structural equivalent lateral stiffness, k_{eq} , can be obtained by

$$k_{eq} = \frac{4\pi^2 W_{eff}}{gT_{eq}^2} \quad (6)$$

where W_{eff} is the effective seismic weight acting on the supporting structure and g is the acceleration of gravity.

Step 5: Computation of Design Base Shear

Using the equivalent lateral stiffness given by Eq. [6], the design process is completed by computing the resulting base shear capacity, V_b , on the supporting structure.

$$V_b = k_{eq} \Delta_t \quad (7)$$

This base shear can then be distributed along the height of the supporting structure per code requirements and used to design the specific structural elements of the supporting structure.

4. Application of Direct Displacement-Based Seismic Design to Nonstructural Elements

The application of the different steps of the direct displacement-based seismic design methodology described in the previous section to nonstructural building elements requires some modifications and the development of new information. Figure 2 presents a flow chart, analogous to Figure 1, illustrating the various steps of the direct displacement-based seismic design process for nonstructural elements. These steps are discussed in this section along with a description of the new information required to apply direct displacement-based seismic design to acceleration-sensitive nonstructural building elements anchored at a single location (floor) of the supporting structure.

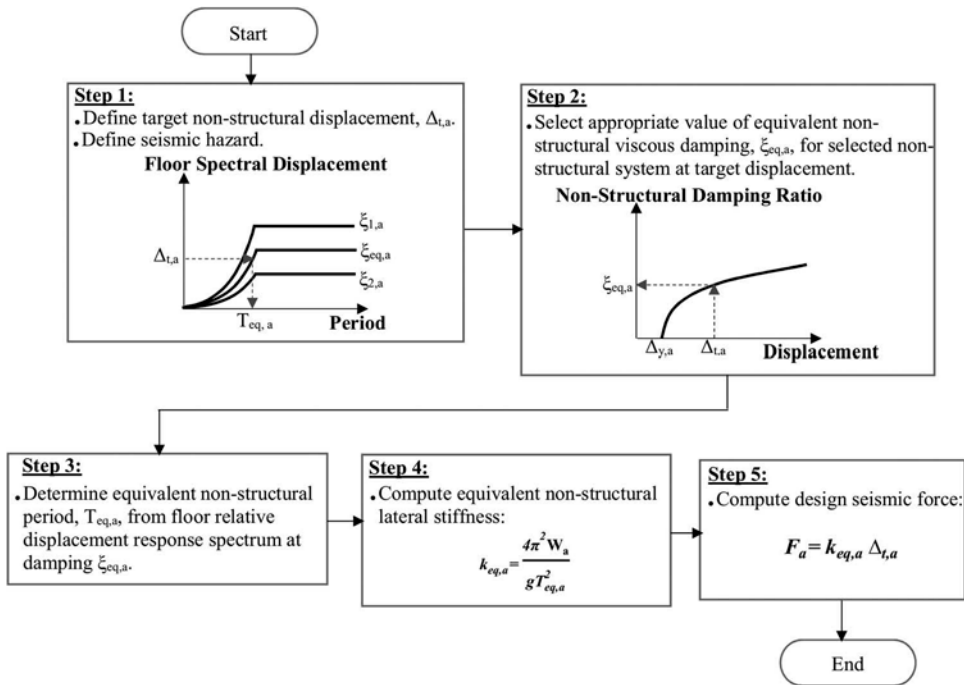


Figure 2. Flowchart of direct displacement-based seismic design of nonstructural building elements.

Step 1: Definition of Target Nonstructural Displacement and Seismic Hazard

The first step in the design procedure is still the definition of the target displacement, $\Delta_{t,a}$, or ductility, $\mu_{t,a}$, that the nonstructural element should not exceed under a given seismic hazard level. This target displacement is associated with the acceptable peak deformation of the nonstructural element relative to its attachment points on the supporting structure for a given seismic hazard level. Note that all sources of deformations in the nonstructural elements (such as supports/anchorage deformations) need also to be considered in the calculation of $\Delta_{t,a}$.

The seismic hazard associated with the target displacement must then be defined in terms of a design floor relative displacement response spectrum, as illustrated in Figure 2. The traditional technique used to calculate a floor response spectrum is first to conduct a dynamic analysis of the supporting structure by itself under a ground motion to calculate the absolute horizontal acceleration time-history of the floor on which the nonstructural element is attached and then to compute the response spectrum of this floor acceleration. If a simplified floor design spectrum needs to be constructed for a given structure, the process needs to be repeated for an ensemble of ground motions representative of the selected design seismic hazard level at the construction site.

Significant efforts have been made in recent years to develop simplified but accurate means of estimating design floor acceleration response spectra [Sullivan *et al.*, 2013; Calvi and Sullivan, 2014; Calvi, 2014; Vukobratović and Fajfar, 2016, 2017]. A simplified method aims to provide, ideally through application of just a few equations, an estimate

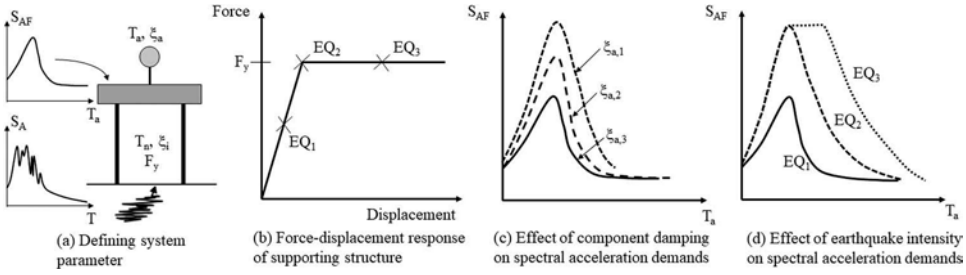


Figure 3. Effects on floor acceleration response spectra (after Sullivan *et al.*, 2013).

of the acceleration spectrum of a floor, S_{AF} , within a supporting structure, such as the SDOF system shown in Figure 3(a), subject to a ground motion for which the acceleration spectrum, S_A , is known. Note that S_A would need to have been modified beforehand for damping and hazard level if necessary (see Eqs. [3] and [4]). In principle, once a floor acceleration spectrum is constructed, the floor relative displacement response spectrum, S_{DF} , can be easily obtained by the usual pseudo-spectra formula [Filiatrault *et al.*, 2013]:

$$S_{DF} = \frac{T_a^2}{4\pi^2} S_{AF} \quad (8)$$

where T_a is the nonstructural period.

As discussed by Sullivan *et al.* [2013], several effects should be accounted when developing design floor acceleration response spectra. These effects are briefly described below and are illustrated in Figure 3.

(i) Effect of dynamic filtering

As shown in Figure 3(c), the seismic waves arriving at a site will tend to be filtered by the structure, with amplification of spectral acceleration demands on nonstructural elements with natural period T_a close to the natural period T_n , of the supporting structure, and reduction of acceleration demands for periods distant from the natural period of the supporting structure. While Figure 3(c) refers to a SDOF system, such filtering can also be expected to occur at the various natural periods of vibration that characterize multi-degree-of-freedom (MDOF) supporting structures.

(ii) Effect of nonstructural damping

The acceleration demand on a nonstructural element will depend on the equivalent viscous damping ratio that characterizes the nonstructural element, ξ_a . This effect is illustrated in Figure 3(c) for three increasing values of nonstructural damping ratio $\xi_{a,1}$, $\xi_{a,2}$, and $\xi_{a,3}$. A simplified method for the construction of floor acceleration spectra should be able to take into account a range of nonstructural damping levels.

(iii) Effect of structural nonlinearity with seismic intensity

The inelastic response of the supporting structure can significantly influence floor acceleration spectra. As the seismic intensity increases, floor spectral acceleration levels will tend to increase. However, at a given seismic intensity, the supporting

structure will undergo inelastic response and will limit the floor spectral accelerations per Newton's second law. If an earthquake ground motion induces inelastic response in the supporting structure, the floor spectral accelerations will saturate over a wider nonstructural period range because of the lengthening of the effective period of the supporting structure. This effect is illustrated in Figure 3(d) for three increasing seismic intensities EQ₁, EQ₂, and EQ₃. Note that the effect of structural nonlinearity on floor acceleration spectra is not easily quantified for MDOF supporting structures because this nonlinearity is different for different modes of vibration [Sullivan *et al.*, 2008].

Considering the above effects, a very simple procedure for the construction of floor acceleration spectra for SDOF supporting structures was developed by Sullivan *et al.* [2013]. The floor acceleration spectrum, S_{AF} , is simply defined by the following simple relations:

$$S_{AF}(T_a) = \frac{T_a}{T_n} \left[a_{\max} \left(\frac{1}{\sqrt{\xi_a}} - 1 \right) \right] + a_{\max} \text{ for } T_a < T_n$$

$$S_{AF}(T_a) = \frac{a_{\max}}{\sqrt{\xi_a}} \text{ for } T_n \leq T_a < T_{eq}$$

$$S_{AF}(T_a) = \frac{a_{\max}}{\sqrt{\left(1 - \frac{T_a}{T_{eq}}\right)^2 + \xi_a}} \text{ for } T_a \geq T_{eq} \quad (9)$$

where a_{\max} is the maximum acceleration of the mass of the supporting structure, which can be easily obtained from the ground response spectrum. Note that a_{\max} saturates at the acceleration level causing yielding of the superstructure, which could be easily considered also by dividing the supporting structure's lateral resistance by its seismic mass. T_n in Eq. [9] is the natural (elastic) period of the supporting structure and ξ_a is the equivalent viscous damping ratio of the nonstructural element. T_{eq} in Eq. [9] is the effective period of the supporting structure, which is equal to the natural period T_n at low intensities and then lengthens with increasing inelastic response brought about by increasing earthquake intensity. If the supporting structure is modeled as an elastic-perfectly plastic SDOF system with no strain-hardening, T_{eq} can easily be obtained by the following:

$$T_{eq} = T_n \text{ for } \mu \leq 1$$

$$T_{eq} = T_n \sqrt{\mu} \text{ for } \mu > 1 \quad (10)$$

where μ is the global displacement ductility ratio exhibited by the supporting structure. For supporting structures with periods of vibration shorter than 0.3 s, the dynamic amplification predicted by Eq. [9] was found to be overestimated and an alternative expression was recommended by Calvi and Sullivan [2014].

Substituting Eq. [9] into Eq. [8] defines completely a design floor relative displacement response spectrum, S_{DF} .

$$S_{DF}(T_a) = \frac{T_a^3}{4\pi^2 T_n} \left[a_{\max} \left(\frac{1}{\sqrt{\xi_a}} - 1 \right) \right] + \frac{T_a^2}{4\pi^2} a_{\max} \text{ for } T_a < T_n$$

$$S_{DF}(T_a) = \frac{T_a^2 a_{\max}}{4\pi^2 \sqrt{\xi_a}} \text{ for } T_n \leq T_a < T_{eq}$$

$$S_{DF}(T_a) = \frac{T_a^2 a_{\max}}{4\pi^2 \sqrt{\left(1 - \frac{T_a}{T_{eq}}\right)^2 + \xi_a}} \leq \frac{T_c^2 a_{\max}}{4\pi^2 \sqrt{\left(1 - \frac{T_c}{T_{eq}}\right)^2 + \xi_a}} \text{ for } T_a \geq T_{eq} \quad (11)$$

For the first, second, and third branches of Eq. [11], S_{DF} varies as a function of $(T_a)^3$, $(T_a)^2$, and T_a , respectively. The third branch of Eq. [11] is capped at a constant value occurring for a corner period T_c . The reason for this limit is that past a corner period, floor displacement spectra tend to stabilize, as pointed out by Calvi [2014]. This corner frequency, however, is difficult to identify for general applications and in the design example discussed later in this paper, it will be assumed that $T_c = T_{eq}$ for simplicity. Even though S_{DF} is expected to drop eventually at long periods to a value corresponding to the peak floor absolute displacement of the supporting structure, considerations relative to this long-period portion of the spectrum are often irrelevant for the seismic design of nonstructural elements, exhibiting much shorter periods of vibration.

To extend the above procedure to MDOF supporting structures responding in the elastic range ($T_{eq} = T_n$), the recommended procedure for floor acceleration spectra proposed by Calvi and Sullivan [2014] can be extended to floor relative displacement response spectra as follows:

- (i) Conduct an elastic modal analysis of the supporting structure and, using the ground response spectrum, determine the acceleration demands expected at level j of the supporting structure for mode of vibration i . These modal peak accelerations, $a_{\max,j,i}$, can be obtained by

$$a_{\max,j,i} = \frac{\phi_{j,i}}{\sum \phi_{j,i} m_j} m_{e,i} S_{A,i} \quad (12)$$

where $\phi_{j,i}$ is the mode shape value at level j for mode i , m_j is the mass of story j , $m_{e,i}$ is the effective mass of mode i , and $S_{A,i}$ is the ground spectral acceleration demand at a period corresponding to mode i .

- (ii) Apply Eq. [12] for each mode of vibration by setting $a_{\max} = a_{\max,j,i}$ in Eq. [11] to obtain the spectral displacements at level j in mode i , $S_{DF,j,i}(T_a)$.
- (iii) For the upper levels (mid-level and above), the floor spectrum can be obtained by taking the square-root-of-the sum-of-the-squares (SRSS) combination of the modal spectral components computed in Step ii.
- (iv) For the lower levels, the predicted floor spectrum can be constructed by taking the larger of the spectral ordinates of either the ground level response spectrum or the spectral accelerations obtained from the SRSS combination of the modal spectral components computed in Step ii.

The above procedure distinguishes between the upper and lower levels of the supporting structure because of the limited filtering that occurs to the ground motion over the lower levels of a structure [see Calvi and Sullivan, 2014 for further details]. In addition, the approach does not define how many modes of vibration need to be considered in Step ii; but for a 20-story reinforced concrete (RC) wall building, Calvi and Sullivan [2014] found that it was sufficient to include only the first three modes of vibration in the direction of excitation under consideration. A rational approach would be to select a number of modes incorporating at least 90% of the total seismic weight of the supporting structure.

Step 2: Determination of Nonstructural Equivalent Viscous Damping

Similar to structural systems, it is necessary to capture the energy dissipation characteristics of the nonstructural element at the target nonstructural displacement, $\Delta_{t,a}$ (or ductility $\mu_{t,a}$), and determine an equivalent viscous damping ratio, $\xi_{eq,a}$. This nonstructural damping database, in the form of a $\xi_{eq,a} - \Delta_{t,a}$ (or $\xi_{eq,a} - \mu_{t,a}$) relationship, must be established from cyclic testing data on the nonstructural typology under consideration. Once this nonstructural damping database has been established, Eq. [5] can be used to determine $\xi_{eq,a}$:

$$\xi_{eq,a} = \frac{E_{D,\Delta_{t,a}}}{2\pi k_{eq,a} \Delta_{t,a}^2} + \xi_{i,a} \quad (13)$$

where $E_{D,\Delta_{t,a}}$ is the energy dissipated per cycle by the nonstructural element at the target displacement, $\Delta_{t,a}$, and $k_{eq,a}$ is the equivalent lateral stiffness of the nonstructural element at the same target displacement. A nominal inherent damping ratio, $\xi_{i,a}$, can also be considered to account for the energy dissipation not associated with the of the nonstructural element hysteretic response.

Step 3: Determination of Nonstructural Equivalent Period

Knowing the target displacement, $\Delta_{t,a}$, and the equivalent viscous damping ratio, $\xi_{eq,a}$, of the nonstructural element at that target displacement, the equivalent (secant) period of the nonstructural element, $T_{eq,a}$, can be obtained directly from the design floor relative displacement response spectrum given by Eq. [11].

Step 4: Computation of Nonstructural Equivalent Lateral Stiffness

Eq. [6] can be used to obtain the nonstructural equivalent lateral stiffness, $k_{eq,a}$, as follows:

$$k_{eq,a} = \frac{4\pi^2 W_a}{g T_{eq,a}^2} \quad (14)$$

where all variables in Eq. [14] have been defined previously.

Step 5: Computation of Design Force

Eq. [7] can then be used to complete the design process by computing the resulting design force, F_a , on the nonstructural element.

$$F_a = k_{eq,a} \Delta_{t,a} \quad (15)$$

This design force can then be applied at the center of mass of the nonstructural element and used to design the specific bracing/anchorage components supporting the

nonstructural element and/or the nonstructural element itself. Note that no iteration on $k_{eq,a}$ is required since the equivalent period of the nonstructural element, $T_{eq,a}$, is obtained directly from the floor response spectrum at the proper damping level and that the operating weight, W_a , and damping ratio, $\xi_{eq,a}$, of the element are known at the design nonstructural displacement $\Delta_{t,a}$. Note again that this approach is limited to nonstructural elements anchored to a single location in the supporting structure.

5. Advantages and Disadvantages of Direct Displacement-Based Seismic Design of Nonstructural Elements

The performance-based seismic design of nonstructural elements using the direct displacement-based strategy, as outlined in the previous section, has the following advantages over the traditional forced-based design procedure discussed in Section 3.

- (1) No estimation of the elastic period of the nonstructural element is required.
- (2) The highly empirical behavior (force reduction) factors (e.g., q_a in Eq. [1]) do not enter the design process.
- (3) Displacements of the nonstructural elements relative to the supporting structure, known to cause the majority of nonstructural damage, drive the design process.

The direct displacement-based seismic design strategy for nonstructural elements, on the other hand, requires detailed knowledge of the variation of the global equivalent nonstructural viscous damping with nonstructural displacement amplitude ($\xi_{eq,a} - \Delta_{t,a}$ relationship). This requirement can be considered a disadvantage of the direct displacement-based design procedure since knowledge of the cyclic behavior of the multitude of nonstructural typologies commonly used in buildings is not well established at this time. To obtain this information, nonstructural system level testing is required in parallel with the development of analytical/numerical models for various nonstructural typologies. These important research activities, however, are not different from those conducted over the last century for structural systems.

Finally, the performance-based seismic design of nonstructural elements using the direct displacement-based strategy can only be implemented once performance objectives, expressed in terms of nonstructural displacements relative to the supporting structures, have been established for various seismic hazards and corresponding ground motion intensities. The establishment of displacement-based performance objectives can also result from the experimental and analytical work outlined above, as well as from reconnaissance surveys following real seismic events.

6. Design Example: Suspended Piping Restraint Installations

To illustrate the application of the direct displacement-based seismic design of acceleration-sensitive nonstructural elements, the design of the seismic restraints for an horizontal mechanical piping system suspended from the top floor of a generic case-study five-story RC building located in a high seismicity site in Italy (near the city of Cassino) is considered in this section. The resulting direct displacement-based seismic design, considering two performance objectives, is also compared to the seismic design obtained by

applying the Eurocode 8 force-based design procedure using current practices. Both designs will be appraised by nonlinear dynamic time-history analyses in the next section.

6.1. Generic Case-Study Building and Site Characteristics

A five-story generic RC office building was considered for the design example. Only one five-story seismic force-resisting frame was designed, as shown in Figure 4. The frame was assumed to be the same in both principal directions of the case-study building. All stories of the frame are 3.5 m in height. The frame was designed using the Eurocode 8 seismic provisions [CEN, 2004] with a force reduction factor $q = 3.75$, corresponding to a ductility class B on a assumed firm ground site near the city of Cassino, Italy, with a design peak ground acceleration (with a return period of 475 years) of 0.21 g. The seismic weight, W_s , of each floor, based on a tributary width of 5 m, along with the dimensions and reinforcement details of the beams and columns are also shown in Figure 4. The concrete strength was assumed to be 30 MPa, while the yield strength of the steel reinforcement was assumed at 450 MPa. An eigenvalue analysis of the designed frame yielded the following first three natural periods based on gross section properties $T_1 = 0.92$ s, $T_2 = 0.33$ s, and $T_3 = 0.21$ s. Figure 5 shows the 5% damped Eurocode 8 design ground acceleration response spectrum ($T_r = 475$ years) for the selected site. Note that the other three spectra shown in the figure will be discussed later in the paper.

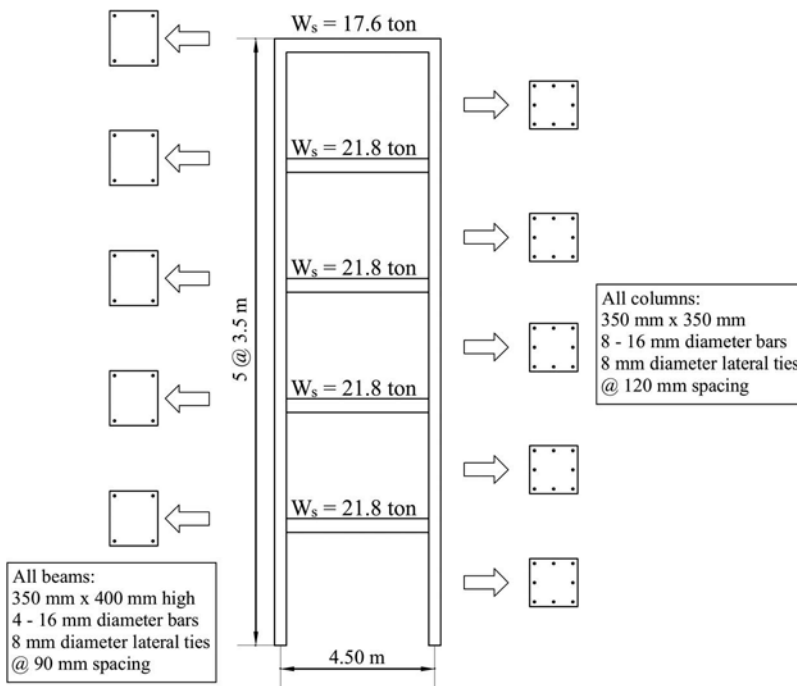


Figure 4. Five-story generic reinforced concrete building considered in design example.

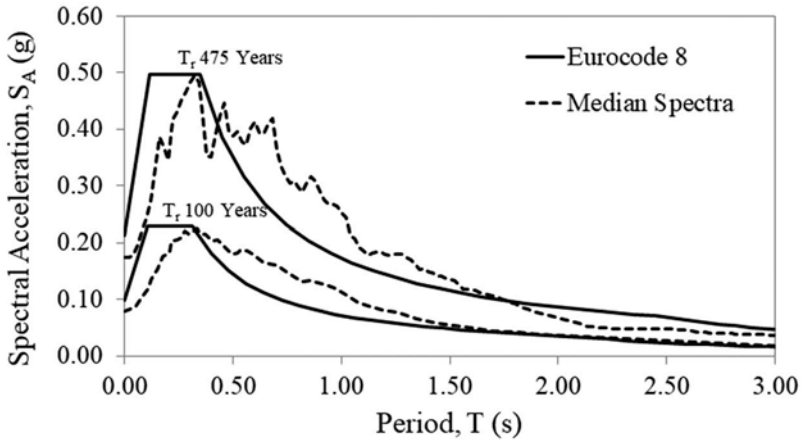


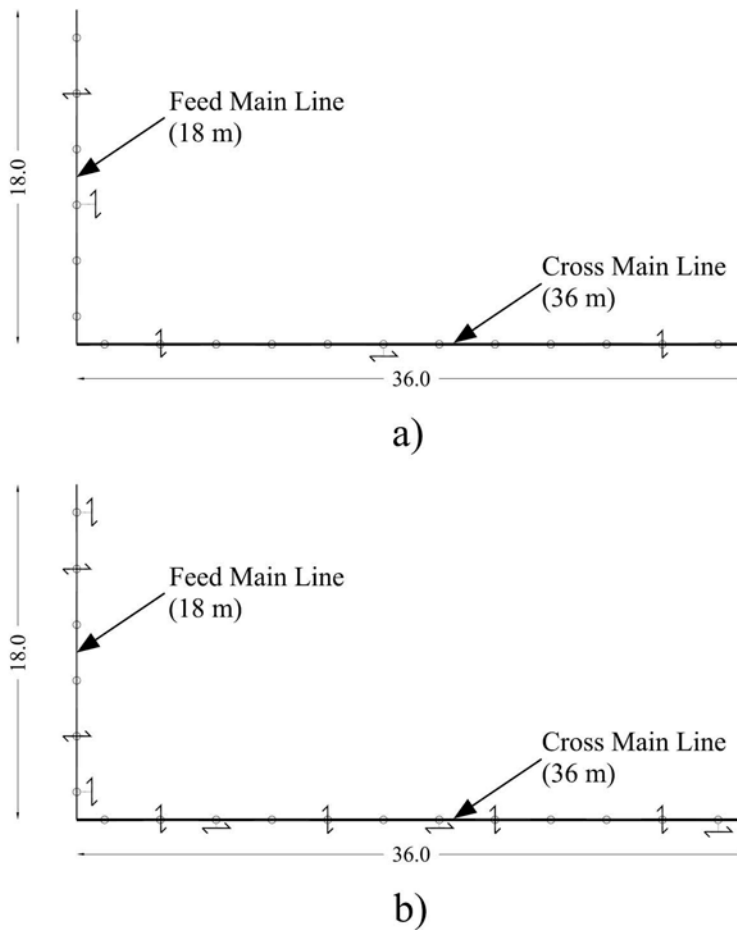
Figure 5. Comparison of ground acceleration 5% damped response spectra for assumed site of case-study building, 475-year and 100-year return periods.

6.2. Mechanical Piping Layout and Properties

The mechanical piping layout selected for the design example was assumed part of the water supply piping system suspended from the top floor of the generic case-study building described in the previous section. Figure 6 shows a plan view of the horizontal piping layout selected. The system includes three separate pipelines: (1) a cold-water distribution line, (2) a hot-water distribution line, and (3) a hot-water recirculation line. The system includes one 18-m-long main feed line connected to a perpendicular 36-m-long cross main line. For simplicity, the effects of the vertical risers and outlets that would connect to the three horizontal pipelines in a real system are neglected. All pipes in the system are assumed to be made of black standard steel with a diameter of 127 mm (5 in) along with a wall thickness of 6.5 mm. All pipe elbows and longitudinal splices are assumed rigidly welded. The unit weight of each water filled pipe, w_a , is equal to 0.31 kN/m.

6.3. Seismic Restraint Configurations and Properties

The pipes are supported by unbraced trapezes used to support vertical gravity loads only (static supports) and sway braced trapezes providing transverse or longitudinal supports. The positions of the vertical static supports are indicated in Figure 6 and are based on a standard static design considering the self-weight of the water filled pipelines. General views and key dimensions of the transverse and longitudinal sway braced trapezes are shown in Figure 7a and b, respectively. For both directions, the vertical supports are provided by a horizontal channel and two vertical steel channels (all 41 mm deep) connected to the top floor slab by rail supports. The vertical channels are connected to the horizontal channel by channel hinges. Each of the three pipes is restrained inside of a pipe ring that is connected to the horizontal channel by a short (50 mm long) vertical 12-mm diameter threaded rod. The transverse and longitudinal seismic restraints are provided by one and two diagonal channels, respectively. Each diagonal channel is oriented at 45° with respect to the vertical and is connected to the ends of the horizontal channel and to the ceiling



Legend:  Static supports  Transverse sway braces  Longitudinal sway braces
All dimensions are in meter

Figure 6. Plan view of mechanical piping layout selected for design example with sway braces according to (a) Eurocode 8 design and (b) direct displacement-based design.

slab by channel hinges. The unbraced trapezes are identical to that shown in Figure 7 but with the diagonal channels omitted.

The design properties for the sway braced trapezes used in this design example are based on the quasi-static cyclic testing conducted by Wood *et al.* [2014] on standard configurations of braced trapezes. The testing was conducted according to the FEMA-461 loading protocol [FEMA, 2007]. The mean properties that are required to conduct the seismic design of the sway braced trapezes were extracted from the test results. These properties are the peak strength, $F_{\max,a}$, yield displacement, $\Delta_{y,a}$, and ductility ratio, μ_a . For the purpose of this design example, the yield displacement, $\Delta_{y,a}$, is defined on the envelope (backbone) force-displacement curve as the intersection between the horizontal line drawn at $F_{\max,a}$ and the secant stiffness at 40% of $F_{\max,a}$. The ductility ratio, μ_a , is defined as the ratio between the ultimate

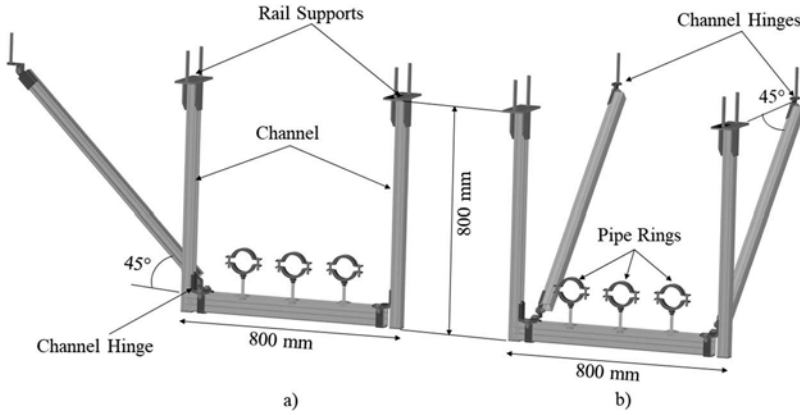


Figure 7. (a) Transverse and (b) longitudinal sway braced trapezes.

Table 1. Mean properties of sway braced trapeze systems.

Direction	Mean properties		
	Peak strength $F_{\max,a}$ (kN)	Yield displacement $\Delta_{y,a}$ (mm)	Ductility ratio μ_a
Transverse	8.6	13.8	1.5
Longitudinal	11.9	18.2	2.5

displacement achieved in the cyclic tests and $\Delta_{y,a}$. Table 1 lists the values of these properties used for the design of the two sway braced trapeze configurations.

6.4. Eurocode 8 Force-Based Seismic Design

The seismic design of the transverse and longitudinal sway braced trapezes is first conducted according to the Eurocode 8 force-based design procedure [CEN, 2004]. For this purpose, the horizontal equivalent static design force, F_a , given by Eq. [1] is applied to each sway braced trapeze over a tributary zone of influence characterized by a spacing, s_a . The design is achieved when the horizontal equivalent static design force is less or equal than the characteristic strength of the sway braced trapeze, F_{Rk} , divided by a resistance factor, γ_m .

$$F_a \leq \frac{F_{Rk}}{\gamma_m} \quad (16)$$

According to Eurocode EN-1990 [CEN, 2002], F_{Rk} should be the 5th percentile characteristic strength, and γ_m depends on the strength variabilities of the sway braced trapeze systems. For simplicity in this design example, F_{Rk} is taken as the mean strength from the Wood *et al.* [2014] tests ($F_{Rk} = F_{\max,a}$ from Table 1) and γ_m is taken equal to 1.25. Substituting Eq. [1] into Eq. [16] and representing the operating weight of the piping, W_a , as the product of the unit weight of the total number of water filled pipes, N_p , (multiplied by a factor of 1.15 to take into account the weight of the fittings and welded connections) and the spacing of the sway braces, s_a , i.e., $W_a = 1.15N_p w_a s_a$, the required spacing of the sway braced trapezes, s_a , can be obtained as follows:

$$s_a \leq \frac{q_a}{\gamma_m \gamma_a S_a} \frac{F_{Rk}}{1.15 N_p w_a} \quad (17)$$

In order to evaluate the seismic coefficient S_a in Eq. [17], the fundamental period of the sway braced trapezes, T_a , must be estimated [see Eq. [2]]. There is significant difficulty in rationally computing the initial periods of nonstructural elements because of the lack of information and guidance in current building codes. The current state of practice for the seismic design of piping seismic restraints is to assume $T_a/T_n = 0$ in Eq. [2]. This simple approach is based on impact hammer tests conducted on a small number of installed field systems that showed fundamental nonstructural periods shorter than 0.1 s [Hilti, 2014]. Note that this approach can be nonconservative as the measured periods may not have been representative of all sources of flexibility in sway braced trapezes (e.g., pipe ring deformations). Furthermore, as discussed above, the use of initial stiffness as an estimate for inelastic components is irrational.

Table 2 summarizes the final seismic design according to the Eurocode 8 force-based design procedure for the transverse and longitudinal sway braced trapezes using a behavior factor $q_a = 2.0$, as specified in Eurocode 8 for suspended systems. The number of required sway braced trapezes in each main line is obtained by dividing the length of piping by the required spacing and rounding up to the highest integer. One transverse and one longitudinal sway braced trapezes are required in the 18-m-long feed main line, while two transverse and one longitudinal sway braced trapezes are required in the 36-m-long cross main line. The resulting sway braced trapeze layout satisfying the Eurocode 8 design is shown in Figure 6(a). Note that the brace spacing values obtained with the Eurocode 8 force-based design procedure (see Table 2) are larger than maximum prescriptive spacing requirements contained in some standards. For example, the Cast Iron Soil Pipe and Fittings Handbook [CISPI, 2006] in the United States suggests a maximum transverse sway brace spacing of 12 m and a maximum longitudinal sway braced trapeze spacing of 24 m for horizontally oriented piping. No such prescriptive spacing requirements are including in nor referenced by the Eurocode 8 and, therefore, are not considered herein.

Table 2. Summary of Eurocode 8 forced-based seismic design for transverse and longitudinal sway brace trapeze systems.

Design parameter	Transverse direction	Longitudinal direction
Number of pipes, N_p		3
Unit weight of one water filled pipe, w_a		0.31 kN/m
Period ratio T_a/T_n , Eq. [17]		0
Design peak ground acceleration, a_g		0.21g
Soil factor, S		1.0
Height ratio, z/H		1.0
Seismic coefficient, S_a , Eq. [2]		0.53
Importance factor, γ_a		1.0
Behavior factor, q_a		2.0
Resistance factor, γ_m		1.25
Characteristic strength, F_{Rk} , Table 1	8.6 kN	11.9 kN
Required spacing of sway braces, s_a , Eq. [17]	24.5 m	33.9 m
Required number of sway braced trapezes in feed main line, $L = 18$ m, Figure 6(A)	1	1
Required number of sway braced trapezes in cross main line, $L = 36$ m, Figure 6(A)	2	1

6.5. Direct Displacement-Based Seismic Design

In this section, the steps described in Section 3 are applied to design the transverse and longitudinal sway braced trapezes according to the proposed direct displacement-based procedure. To illustrate the flexibility of the procedure, two different performance objectives linked to different ground motion return periods are considered. These two performance objectives and ground motion return periods are summarized in Table 3.

The first performance objective is associated with damage prevention in the sway braced trapezes under frequent earthquakes having a return period $T_r = 100$ years. For this example, the damage prevention performance objective is assumed to be associated with a target displacement equal to the yield displacements, $\Delta_{y,a}$, of the sway braced trapezes, as listed in Table 1 for the transverse and longitudinal directions, respectively. The associated target ductility ratio of the sway braced trapezes is, therefore, $\mu_{t,a} = 1.0$ in both directions. The second performance objective is associated with life-safety prevention under design earthquakes with a return period $T_r = 475$ years. For this example, the life-safety prevention performance objective is also associated with collapse prevention of the sway braced trapezes and is assumed to be associated with the maximum ductility ratio achieved in the cyclic tests conducted by Wood *et al.* [2014], μ_a , as listed in Table 1 for the transverse and longitudinal directions, respectively. Therefore, the associated life-safety prevention target ductility ratios of the sway braced trapezes are $\mu_{t,a} = 1.5$ and 2.5 in the transverse and longitudinal directions, respectively. Note that the two performance objectives considered for this example are only for illustration of the proposed direct displacement-based seismic design methodology. Multiple performance objectives could be considered in a real design situation provided that a target displacement of the sway braced trapezes can be associated with each performance objective.

Equation [16] still applies to the direct displacement-based seismic design except that the horizontal equivalent design force to each sway braced trapeze, F_a , is obtained by Eq. [15]. Substituting Eq. [14] and Eq. [15] into Eq. [16], the required spacing of the sway braced trapezes, s_a , can be obtained as follows:

$$s_a \leq \frac{gT_{eq,a}^2}{4\pi^2\Delta_{t,a}} \frac{F_{Rk}}{1.15\gamma_m N_p w_a} \quad (18)$$

where all variables in Eq. [18] have been defined previously.

Recall that $T_{eq,a}$ in Eq. [18] is the equivalent (secant) period of the sway braced trapezes that can be obtained from the design floor relative displacement response spectrum, knowing the target displacement, $\Delta_{t,a}$, and the equivalent viscous damping ratio, $\xi_{eq,a}$, of the sway braced trapezes at that target displacement. To establish the required $\xi_{eq,a} - \Delta_{t,a}$

Table 3. Performance objectives for direct displacement-based seismic design of transverse and longitudinal sway brace trapeze systems.

Performance objective	Ground motions return period, T_r (year)	Sway braced trapeze target displacement, $\Delta_{t,a}$ (mm)		Sway braced trapeze target ductility ratio, $\mu_{t,a}$	
		Transverse direction	Longitudinal direction	Transverse direction	Longitudinal direction
Damage prevention	100	13.8	18.2	1.0	1.0
Life-safety/collapse prevention	475	20.7	45.5	1.5	2.5

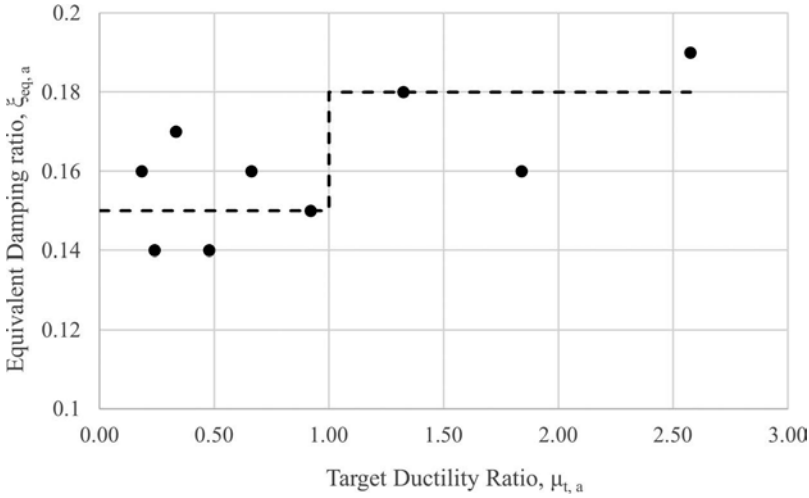


Figure 8. Variation of equivalent viscous damping ratio with target ductility ratio.

(or $\xi_{eq,a} - \mu_{t,a}$) relationship, Eq. [13] was applied at each displacement amplitude of the hysteretic curves from the cyclic tests on sway braced trapezes conducted by Wood *et al.* [2014] and described in Section 6.3. Figure 8 shows the resulting $\xi_{eq,a} - \mu_{t,a}$ data extracted from the tests along with a very simple model (shown with dotted lines) adopted for this design example:

$$\begin{aligned} \xi_{eq,a} &= 0.15 \text{ for } \mu_{t,a} \leq 1.0 \\ \xi_{eq,a} &= 0.18 \text{ for } \mu_{t,a} > 1.0 \end{aligned} \quad (19)$$

The apparent high damping value ($\xi_{eq,a} = 0.15$) for $\mu_{t,a} \leq 1$ in Eq. [19] is the result of the sway braced trapezes tested by Wood *et al.* [2014] exhibiting hysteretic energy dissipation characteristics over their entire displacement ranges without a clear elastic region.

To construct the design top (fifth) floor relative displacement response spectra, S_{DF} , for the case-study building, Eq. [11] can be used. Although the case-study building would be expected to undergo inelastic actions under design ($T_r = 475$ years) ground motions, this inelastic action would affect only the second and third branches of the floor relative displacement spectrum at periods longer than the expected equivalent (secant) period of the sway braced trapezes, $T_{eq,a}$. For simplicity, the case-study building was assumed to remain elastic for both ground motion intensities considered ($T_r = 100$ and 475 years) and, thereby, it was assumed that $T_c = T_{eq} = T_n = 0.92$ s in Eq. [11]. The first three modes of vibration of the case-study building were considered to construct the top floor relative displacement response spectra per the methodology proposed by Calvi and Sullivan [2014], described in Section 4. For each ground motion intensity, the modal top (fifth) floor peak horizontal accelerations, $a_{max,5,j}$, were calculated by Eq. [12]. The design ground spectral acceleration demand for each of the first three modes of vibration of the case-study building, $S_{A,j}$, was obtained by consulting the Eurocode 8 design ground acceleration response spectrum shown in Figure 5. Table 4 summarizes the calculations of the modal peak accelerations at the top floor of the case-study building for the design ground

Table 4. Summary modal peak acceleration calculations at top floor of case-study building for design ground motions intensity ($T_r = 475$ years).

Mode i	Natural period T_i (s)	Ground spectral acceleration, $S_{A,i}$ (g)	Effective modal mass $m_{e,i}$ (t)	Cumulative percentage of total seismic mass	Mode shape value at level 5, $\phi_{5,i}$	$\sum \phi_{j,i} m_j$ (t) Eq. [12]	Modal peak accelerations at level 5
		Figure 5					$a_{max,5,i}$ (g) Eq. [12]
1	0.92	0.27	86.0	82	0.14	9.23	0.36
2	0.33	0.44	11.32	93	0.12	3.79	0.16
3	0.21	0.35	4.57	97	0.11	1.79	0.10

motions intensity ($T_r = 475$ years). The first three modes of vibration of the case-study building incorporate 97% of its total seismic weight. The modal peak accelerations at the top floor of the case-study building for the ground motions intensity associated with damage prevention ($T_r = 100$ years) were obtained by scaling the values shown in Table 4 by a factor of 0.507 obtained from the seismic hazard curve at the site [Barani *et al.*, 2009].

Figure 9 shows the resulting design top (fifth) floor relative displacement response spectra for the case-study building. The spectra are plotted for equivalent viscous damping ratios of 15% and 18% of critical according to Eq. [19]. These floor relative displacement response spectra can then be used to complete the seismic design of the sway braced trapezes according to the proposed direct displacement-based procedure, as summarized in Table 5. As expected, the range of sway braced trapeze equivalent periods, $T_{eq,a}$, listed in Table 5 (0.36–0.53 s) is significantly longer than elastic periods, T_a , estimated from low amplitude impact hammer tests [Hilti, 2014]. Basing the seismic design on realistic equivalent (secant) period of vibrations is one of the main strengths of the direct displacement-based seismic design procedure. The resulting spacing of the sway braced trapezes from the direct displacement-based seismic design procedure for both the transverse and longitudinal directions is governed by the life-safety prevention performance objective for ground motions having a return period $T_r = 475$ years. Again here, the number of required sway braced trapezes in each main line is obtained by dividing the

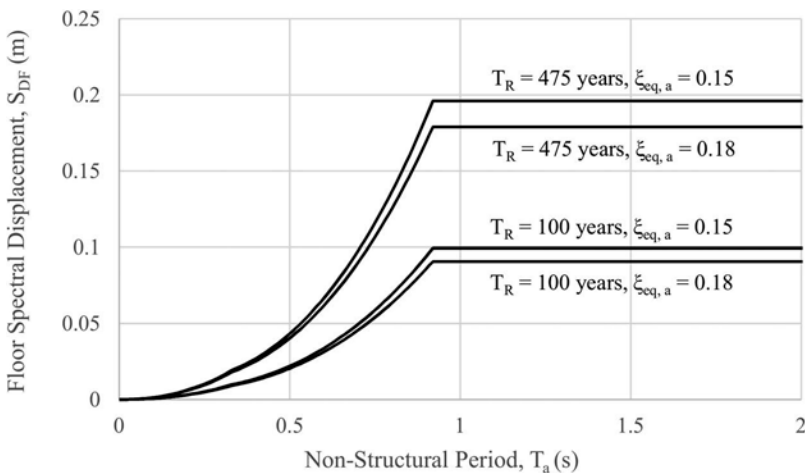


Figure 9. Design top floor relative displacement response spectra for case-study building.

Table 5. Summary of direct displacement-based seismic design for transverse and longitudinal sway braced trapeze systems.

Design parameter	Final design values			
	Damage prevention hazard level, $T_r = 100$ years		Safety prevention hazard level, $T_r = 475$ years	
	Transverse	Longitudinal	Transverse	Longitudinal
Sway braced trapeze target ductility ratio, $\mu_{t,a}$	1.0	1.0	1.5	2.5
Sway braced trapeze target displacement, $\Delta_{t,a}$ (mm), Table 3	13.8	18.2	20.7	45.5
Sway braced trapeze equivalent viscous damping ratio, $\xi_{eq,ar}$ Eq. [19]		0.15		0.18
Sway braced trapeze equivalent period, $T_{eq,ar}$ Figure 9	0.40 s	0.46 s	0.36 s	0.53 s
Number of pipes, N_p			3	
Unit weight of one water filled pipe, w_a			0.31 kN/m	
Resistance factor, γ_m			1.25	
Characteristic strength, F_{Rk} Table 1	8.6 kN	11.9 kN	8.6 kN	11.9 kN
Required spacing of sway braces, s_a , Eq. [18]	18.5 m	25.7 m	10.0 m	13.7 m
Required number of sway braced trapezes in feed main line, $L = 18$ m, Figure 6(b)	1	1	2*	2*
Required number of sway braced trapezes in cross main line, $L = 36$ m, Figure 6(b)	2	2	4*	3*

*Control the design.

length of piping by the required spacing and rounding up to the highest integer. Two transverse and two longitudinal sway braced trapezes are required in the 18-m-long feed main line while four transverse and three longitudinal sway braced trapezes are required in the 36-m-long cross main line. The layout of the sway braced trapezes satisfying the proposed direct displacement-based seismic design procedure is shown in [Figure 6\(b\)](#). Clearly, the direct displacement-based design results in more sway braced trapezes than that obtained by the Eurocode 8 force-based design procedure discussed in the previous section, which should yield better seismic performance.

7. Design Example Appraisal

In this section, the seismic performance of the transverse and longitudinal sway braced trapezes designed according to the Eurocode 8 approach, discussed in [Section 6.4](#), is compared to that of the seismic design conducted according to the proposed direct displacement-based procedure, described in [Section 6.5](#). An ensemble of ground motions was first generated for each of the two design return periods ($T_r = 100$ and 475 years) considered at the site of the case-study building. Using these two ensembles of ground motions, two-dimensional nonlinear time-history (NLTH) dynamic analyses were conducted on the case-study building to generate an ensemble of top floor input motions for each of the same two return periods. Using these top floor input motions, three-dimensional NLTH dynamic analyses were in turn conducted on the mechanical piping system incorporating the transverse and longitudinal sway braced trapeze layouts resulting from the Eurocode 8 design and from the direct displacement-based seismic design procedure ([Figure 6](#)). Finally, cumulative probability distributions of the maximum relative transverse and longitudinal displacements between the sway braced trapezes and the supporting structure were generated to evaluate the probability of exceedance of the target

displacements associated with the performance objectives considered for the two ground motion return periods, thereby appraising the two different design methodologies.

7.1. Selection of Earthquake Ground Motions

A set of 20 three-dimensional ground motions representative of earthquake ground motions at the site of the case-study building for both design return periods ($T_r = 100$ and 475 years) were selected from the PEER NGA-West database [PEER, 2018].

In this study, a site close to the city of Cassino in Italy was chosen for the ground motions selection. As described in Section 6.5, the site is characterized by a peak ground acceleration on stiff soil equal to 0.21 g for a return period $T_r = 475$ years. The corresponding peak ground acceleration for a return period $T_r = 100$ years is 0.10 g based on the hazard curve for the site [Barani *et al.*, 2009]. Hazard-consistent record selection was based on spectral compatibility (matching of the geometric mean) with a conditional mean spectrum according to the methodology proposed by Jayaram *et al.* [2011]. For this study, the conditioned period of interest was selected to be 1.0 s because it is near the fundamental period of the case-study building (0.92 s).

Figure 5 compares the median response spectrum obtained from the two horizontal components of the 20 considered ground motions (40 horizontal records) with the Eurocode 8 design response spectrum for return periods of 100 and 475 years, respectively. Good agreement is observed between the median and Eurocode peak spectral values. The median spectral values envelope the Eurocode 8 design spectra in the range of the first three elastic natural periods of the case-study building (0.21–0.92 s).

7.2. Modeling of Case-Study Building

The nonlinear model of the case-study frame shown in Figure 4 is based on a lumped plasticity approach with the OpenSees software [Mazzoni *et al.*, 2006]. The interaction between the structural and other nonstructural elements was neglected in this cascading approach. The primary structural elements were modeled by elastic beam and column elements with plastic rotational hinges at both ends. The yielding and ultimate end rotations were determined according to Eurocode 8 procedures [CEN, 2004]. The hysteretic behavior of each plastic hinge was simulated using the Pinching4 uniaxial material model available in OpenSees. The moment-rotation backbone curve was composed of four branches describing (1) the first cracking of the concrete, (2) the yielding of the longitudinal bars, (3) the maximum flexural capacity of the section, and (4) the residual moment capacity assumed arbitrarily equal to 20% of the maximum flexural capacity [Rozman and Fajfar, 2009]. The well-known Takeda model [Takeda *et al.*, 1970] was used to simulate the hysteretic response of the plastic hinges.

The axial forces in the beams were neglected but the yield moments in the columns were adjusted at each time-step based on axial load-bending moment interaction curves. The bases of the first floor columns were assumed fixed and the foundation assumed to be rigid. As shown in Figure 4, the seismic weight of each floor was taken equal to 21.8 t except for the top level, which was taken as 17.6 t. Large-displacement nonlinear dynamic response analyses were conducted using Newmark's explicit integration scheme with an integration time-step equal to the time-step of each horizontal earthquake record divided by 10. Rayleigh tangent stiffness proportional viscous damping was introduced in the

numerical model with 5% of critical damping specified in the first mode of vibration. The first three elastic natural periods of the structure ($T_1 = 0.92$ s, $T_2 = 0.33$ s, and $T_3 = 0.21$ s) were already provided in [Section 6.1](#).

7.3. Generation of Top Floor Input Motions

Nonlinear time-history dynamic analyses of the case-study frame were conducted using the 20 horizontal ground motion pairs (40 records) generated for each of the return periods considered ($T_r = 100$ and 475 years). [Figure 10](#) compares the median 5% damped capacity response spectra (i.e., $S_{AF}(T_a)$ vs. $S_{DF}(T_a)$) for the 40 horizontal top floor acceleration components along with the corresponding response spectra predicted by Eq. [9] and Eq. [11], which were used for the seismic design of the swayed braced trapezes of the mechanical piping system. The spectra predicted by Eq. [9] and Eq. [11] match very well the median floor motions spectra over the first three natural periods of the case-study building. For periods longer than the fundamental period of the case-study building (0.92 s), Eq. [11] caps the spectral displacement to a constant value, while the floor motions median spectra reduce toward the peak floor absolute displacements of the supporting structure. Note that the slight fundamental period lengthening due to the inelastic response of the supporting structure under 475-year ground motions can be observed in [Figure 10\(b\)](#) for the median floor capacity spectrum.

The mechanical piping system was analyzed under three-dimensional top floor motions. For each return period, the horizontal floor motion components obtained on the top floor of the case-study building were combined to create 20 horizontal floor motions pairs. Since the mechanical piping system is a spatial structure that can be oriented in any of the two principal directions of the supporting case study building, the horizontal components were then rotated 90° from each other to create 40 horizontal floor acceleration pairs. The vertical acceleration component of each ground motion selected was scaled similarly to the horizontal components and used directly at the top level of the case-study building to create 40 three-dimensional floor motions for the three-dimensional nonlinear dynamic response analyses of the mechanical piping system. It was assumed that the case-study building behaved as a rigid body in the vertical direction with no amplification of the vertical ground motions.

7.4. Modeling of Piping Systems

Three-dimensional models of the two design alternatives of the sway braced water piping system shown in [Figure 6](#) were developed in OpenSees for calculating their dynamic responses under the triaxial floor motions generated in the previous section. All pipes were modeled as elastic frame elements in the same horizontal plane located at a drop height of 800 mm from the top slab of the case-study building. All nodes were free to deform in translations and rotations except at the locations of vertical gravity load trapezes (static supports), where vertical translations were constrained. The longitudinal and transverse sway braced trapezes were modeled by horizontal nonlinear springs in their

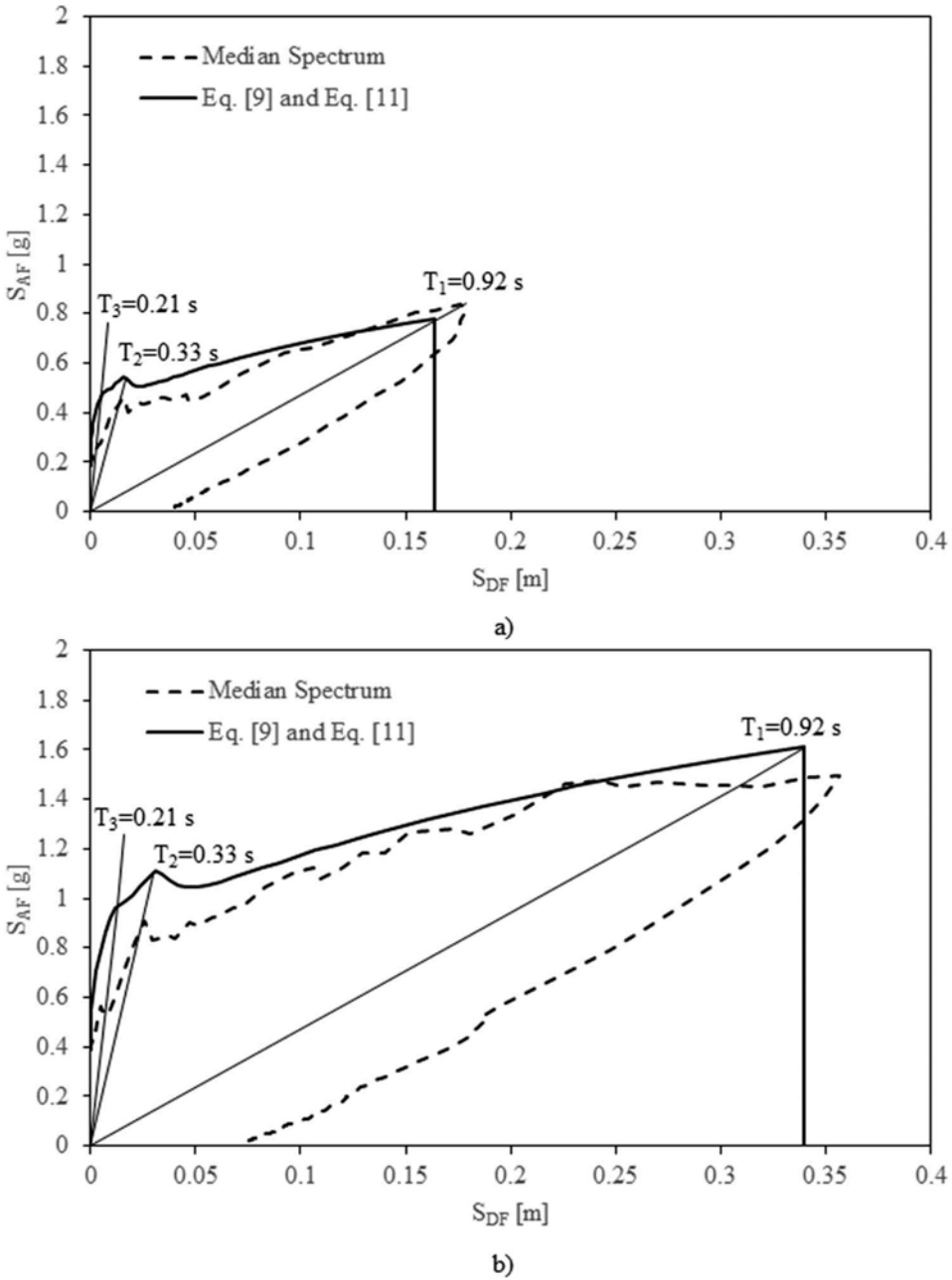


Figure 10. Comparisons of 5% damped median capacity response spectra for 40 horizontal top floor acceleration components and response spectra predicted by Eq. [9] and Eq. [11]; (a) return period $T_r = 100$ years, (b) return period $T_r = 475$ years.

bracing directions between the piping and top slab-based nodes using the Pinching4 uniaxial material model available in OpenSees. The hysteretic properties of each Pinching4 hysteretic spring were obtained by fitting the global force–displacement relationship obtained from the quasi-static cyclic testing conducted by Wood *et al.* [2014] and

described in Section 6.3. The horizontal and vertical masses of the water filled pipes were lumped at each node based on tributary widths. Beyond the explicit hysteretic damping provided by the sway bracing hysteretic springs, a small amount (2% of critical) of Rayleigh type viscous damping was assigned based on the first and third elastic modes of vibration of each numerical model.

7.5. Analysis Results

The first three elastic natural periods and mode shapes predicted by the numerical models of the two-design alternatives of the mechanical piping model are shown in Figure 11. Due to the high bending stiffness of the three 5-in black standard steel piping compared to that of the sway braced trapezes, the mode shapes predicted by the numerical models are global modes with most of the deformations in the sway braced trapezes and with the piping behaving essentially as a rigid body. The elastic fundamental periods calculated for the two-design alternatives ($T_1 = 0.41$ s for the Eurocode 8 design and $T_1 = 0.27$ s for the

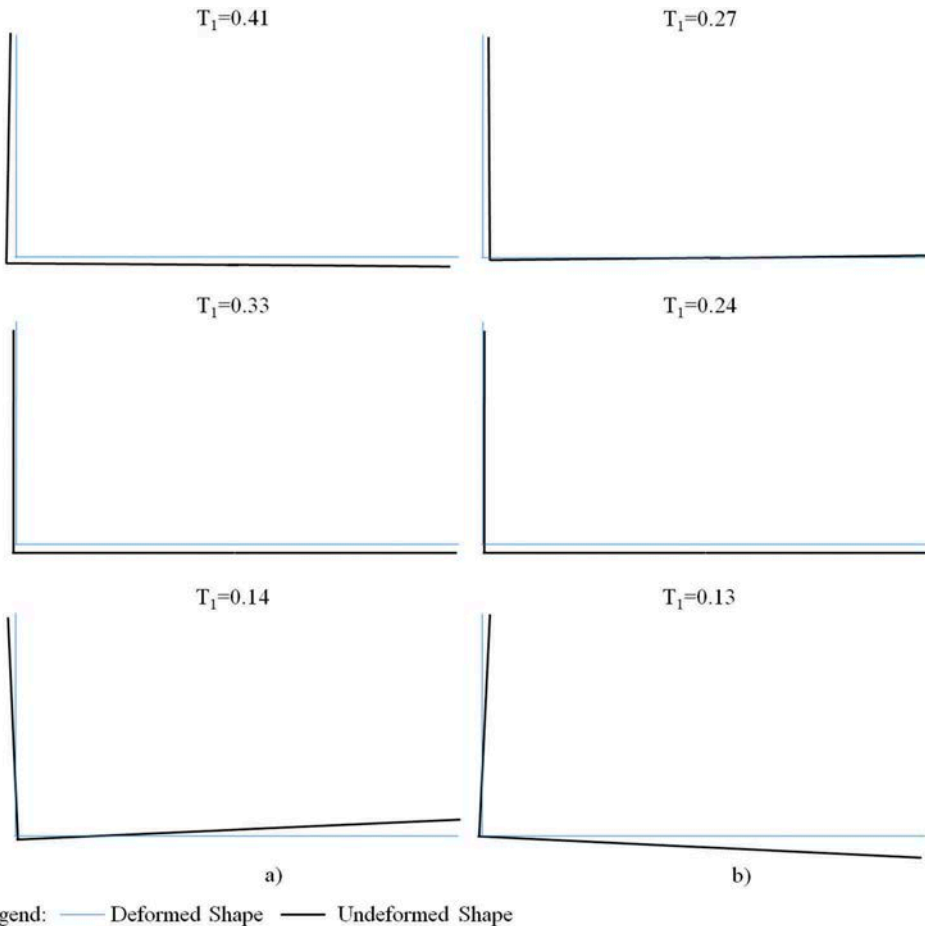
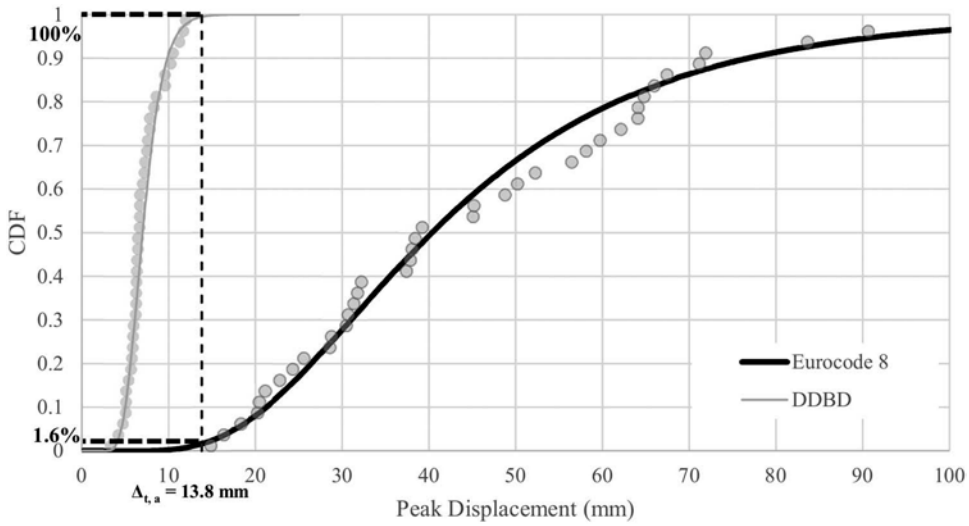
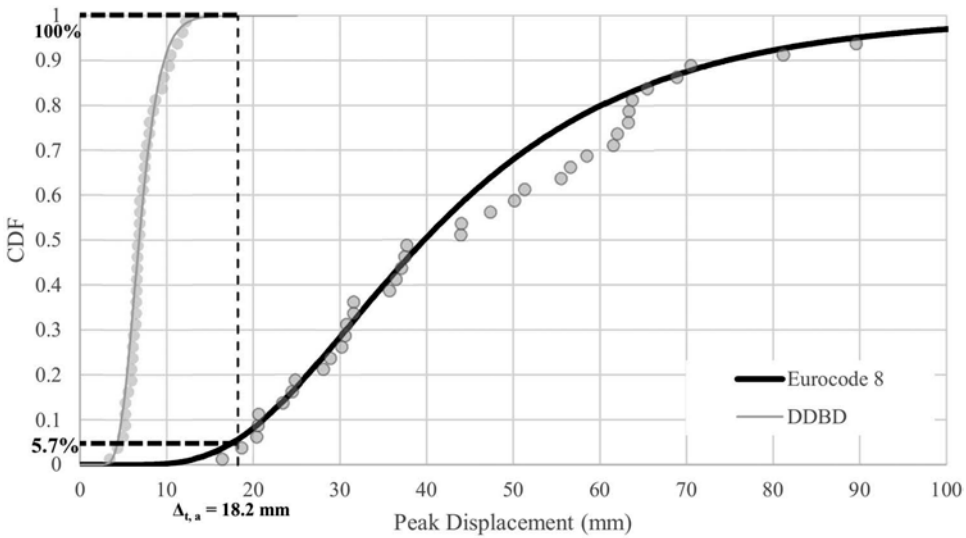


Figure 11. Natural periods and mode shapes computed for mechanical piping systems designed according to (a) Eurocode 8 design and (b) direct displacement-based design.



a)

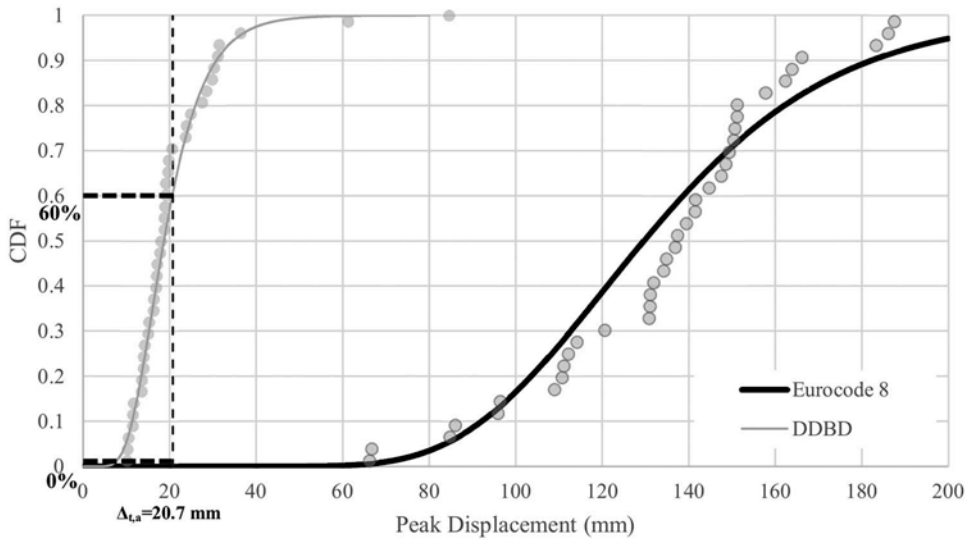


b)

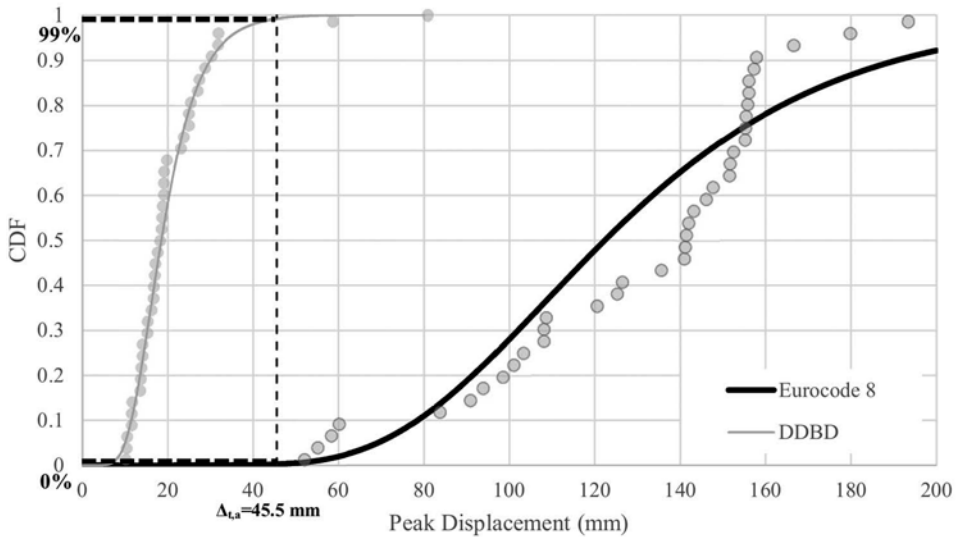
Figure 12. Cumulative distribution functions (CDFs) for peak transverse and longitudinal displacements in sway braced trapezes for Eurocode 8 design and direct displacement-based design (DDBD), $T_r = 100$ years, (a) transverse direction and (b) longitudinal direction.

direct displacement-based design) are significantly longer than 0.1 s, as obtained from impact hammer tests [Hilti, 2014]. These results put in doubt the practice of using $T_a/T_n = 0$ in the force-based Eurocode 8 design procedure (Eq. [2]).

Figures 12 and 13 show cumulative distribution functions (CDFs) for the peak transverse and longitudinal displacements in the sway braced trapezes for the two-design



a)



b)

Figure 13. Cumulative distribution functions (CDFs) for peak transverse and longitudinal displacements in sway braced trapezes for Eurocode 8 design and direct displacement-based design (DDBD), $T_r = 475$ years, (a) transverse direction and (b) longitudinal direction.

alternatives (Eurocode 8 and direct displacement-based) and for ground motion return periods $T_r = 100$ and 475 years, respectively. The empirical CDF data shown in each graph were fitted with a lognormal CDF following the procedure proposed by Baker [2015]. The target displacements associated with each of the two performance objectives considered (Table 3) are indicated by vertical dashed lines in each plot along with their associated

Table 6. Parameters for lognormal cumulative distribution functions of maximum displacements in transverse and longitudinal directions for Eurocode 8 and direct displacement-based designs and for ground motion return periods $T_r = 100$ and 475 years.

	$T_r = 100$ years				$T_r = 475$ years			
	Transverse direction		Longitudinal direction		Transverse direction		Longitudinal direction	
	Eurocode 8	DDBD*	Eurocode 8	DDBD*	Eurocode 8	DDBD*	Eurocode 8	DDBD*
Median (mm)	40.3	6.8	39.7	6.9	129.6	18.7	122.3	18.5
β	0.50	0.28	0.49	0.27	0.27	0.39	0.35	0.38

*Direct displacement-based design.

Table 7. Lognormal probabilities of exceedance of target displacements, $P[E/\Delta_{t,a}]$, in transverse and longitudinal directions for Eurocode 8 and direct displacement-based designs and for ground motion return periods $T_r = 100$ and 475 years.

$P[E/\Delta_{t,a}]$							
$T_r = 100$ years				$T_r = 475$ years			
Transverse direction		Longitudinal direction		Transverse direction		Longitudinal direction	
Eurocode 8	DDBD*	Eurocode 8	DDBD*	Eurocode 8	DDBD*	Eurocode 8	DDBD*
98.4%	0.0%	94.3%	0.0%	100.0%	40.0%	100.0%	1.0%

*Direct displacement-based design.

lognormal percentiles, $LNP/\Delta_{t,a}$. The lognormal probability of exceedance of each target displacement, $P[E/\Delta_{t,a}]$, can then be simply obtained by

$$P[E/\Delta_{t,a}] = 1 - [LNP/\Delta_{t,a}] \quad (20)$$

Table 6 lists the median and lognormal standard deviation, β , values for all the computed lognormal CDFs. The β values listed in the table capture only the floor motions variability arising from the ground motions record-to-record variability. Table 7 summarizes the lognormal probabilities of exceedance of the target displacements in the transverse and longitudinal directions for both design alternatives and for both design ground motion return periods.

The sway braced trapezes designed according to the Eurocode 8 force-based design procedure fail to meet the target displacements in both directions and for both design ground motions return periods. For the 475-year return period, the median peak displacements obtained with the Eurocode 8 force-based design procedure exceed the target displacements by 109 mm (6.3 times) and 77 mm (2.7 times) in the transverse and longitudinal directions of the sway braced trapezes, respectively. The corresponding values for the 100-year return period are 27 mm (2.9 times) and 22 mm (2.2 times) in the transverse and longitudinal directions of the sway braced trapezes, respectively. The resulting lognormal probabilities of exceedance of the target displacements are essentially 100% for the 475-year return period, as listed in Table 7. This poor performance of the Eurocode 8 design is the direct result of the $T_a/T_n = 0$ assumption in Eq. [2]. Other assumptions could have resulted in complete different designs and performances. For example, if $T_a/T_n = 1$ is used in Eq. [2], the spacing of the sway braced trapezes for the 475-year return period would be 11.1 and 15.4 m in the transverse and longitudinal direction, respectively. These spacing values are very close to that obtained with the direct displacement-based design (see Table 5). This illustrates the incoherence in using empirical forced-based seismic design procedures.

The sway braced trapezes designed according to the proposed direct displacement-based procedure, on the other hand, meet the target displacements in both directions and for both design ground motions return periods. For the 475-year return period, the median peak displacements obtained from the direct displacement-based design procedure underpredict the target displacements by only 2 and 27 mm in the transverse and longitudinal directions of the sway braced trapezes, respectively. The corresponding values for the 100-year return period are 7 and 11 mm in the transverse and longitudinal directions of the sway braced trapezes, respectively. The resulting lognormal probabilities of exceedance of the target displacements are nearly 0% except for the 475-year return period in the transverse direction, as listed in Table 7. For this governing design case (see Table 5), one would expect the median displacement to be close to the target displacement. The results shown in Table 7 indicate that the probability of exceedance of the target displacement for the 475-year return period in the transverse direction of the sway braced trapezes is 40%, which is close to the 50% probability of exceedance associated with the median displacement. These results illustrate the coherence in using the much more rational direct displacement-based design procedure.

8. Conclusions

A framework for the application of direct displacement-based seismic design to nonstructural building elements has been developed in this paper. The proposed design procedure applies mainly to acceleration-sensitive nonstructural elements suspended or anchored at a single location (floor) in the supporting structure and for which damage is the result of excessive displacements (e.g., piping systems, cable trays, suspended ceilings, etc.).

A numerical example of the direct displacement-based seismic design of a horizontal mechanical piping system suspended from the top floor of a generic case-study and code-designed five-story RC building located in a high seismicity site in Italy was presented and compared with the force-based design procedure of Eurocode 8 using current practices. Both design alternatives were evaluated through nonlinear time-history dynamic analyses using floor motions generated from earthquake records representative of two hazard levels that were associated with two different design performance levels. The results showed that the proposed direct displacement-based seismic design procedure satisfied well the performance objectives, while the Eurocode 8 design did not.

The proposed direct displacement-based seismic design strategy for nonstructural elements requires detailed knowledge of the variation of the global equivalent nonstructural viscous damping with nonstructural displacement amplitude. Knowledge of the cyclic behavior of the multitude of nonstructural typologies commonly used in buildings is not well established at this time. To obtain this information, nonstructural system level testing is required in parallel with the development of analytical/numerical models for various nonstructural typologies. These important research activities are similar to those conducted over the last century for structural systems.

Beyond the need to develop a robust experimental nonstructural hysteretic database, much future work is required to generalize the proposed direct displacement-based seismic design methodology for nonstructural elements. For example, the methodology should be expanded to nonstructural elements with multiple attachment points in the supporting structure. Also, correction factors to equivalent nonstructural viscous damping values used in the direct displacement-based procedure need to be established to better

represent the actual nonlinear seismic response of a variety of nonstructural element typologies. Finally, some more work is required to develop a general simplified procedure to construct design floor relative displacement response spectra.

Acknowledgments

The work presented in this paper has been developed within the framework of the project “Dipartimenti di Eccellenza” at the University School for Advanced Studies IUSS Pavia.

Funding

The work was funded by the Italian Ministry of Education, University and Research.

References

- ASCE. [2016] *ASCE 7-16: Minimum Design Loads for Buildings and Other Structures*, American Society of Civil Engineers, Reston, Virginia. pp. 889.
- ASCE. [2017] *ASCE/SEI 41-17: Seismic Evaluation and Retrofit of Existing Buildings*, American Society of Civil Engineers, Structural Engineering Institute, Reston, Virginia. pp. 576.
- Baker, J. W. [2015] “Efficient analytical fragility function fitting using dynamic structural analysis,” *Earthquake Spectra* **31**(1), 579–599. doi:10.1193/021113EQS025M.
- Barani, S., Spallarossa, D. and Bazzurro, P. [2009] “Disaggregation of probabilistic ground-motion hazard in Italy,” *Bulletin of the Seismological Society of America* **99**, 2638–2661. doi:10.1785/0120080348.
- Calvi, P. [2014] “Relative displacement floor spectra for seismic design of non structural elements,” *Journal of Earthquake Engineering* **18**, 1037–1059. doi:10.1080/13632469.2014.923795.
- Calvi, P. M. and Sullivan, T. J. [2014] “Estimating floor spectra in multiple degree of freedom systems,” *Earthquakes and Structures, an International Journal Techno Press* **6**(7), 17–38. doi:10.12989/eas.2014.7.1.017.
- CEN. [2002] *EN-1990: 2002+A1: Eurocode - Basis of Structural Design*, Comité Européen de Normalization, Brussels, Belgium.
- CEN. [2004] *EN-1998-1:2004: E: Eurocode 8 – Design Provisions for Earthquake Resistant Structures*, Comité Européen de Normalization, Brussels, Belgium.
- Chock, G., Robertson, I., Nicholson, P., Brandes, H., Medley, E., Okubo, P., Hirshorn, B., Sumada, J., Kindred, T., Linurna, G., Sarwar, A., Dal Pino, J. and Holmes, W. [2006] *Compilation of Observations of the October 15, 2006, Kiholo Bay (M_w 6.7) And Mahukona (M_w 6.0) Earthquakes, Hawaii*, Earthquake Engineering Research Institute, Oakland, California. pp. 53.
- CISPI. [2006] *Cast Iron Soil Pipe and Fittings Handbook*, Cast Iron Soil Pipe Institute, Chattanooga, Tennessee, pp. 218.
- Drake, R. M. and Bachman, R. E. [1996] “NEHRP Provisions for 1994 for non-structural components,” *Journal of Architectural Engineering American Society of Civil Engineers* **2**(1), 26–31. doi:10.1061/(ASCE)1076-0431(1996)2:1(26).
- Dwairi, H. M., Kowalsky, M. J. and Nau, J. M. [2007] “Equivalent damping in support of direct displacement-based design,” *Journal of Earthquake Engineering* **11**(4), 512–530. doi:10.1080/13632460601033884.
- Ercolino, M., Petrone, C., Coppola, O. and Magliulo, G. [2012] “Report sui danni registrati a San Felice sul Panaro (Mo) in seguito agli eventi sismici del 20 e 29 maggio 2012 – v1.0,” available online: <http://www.reluis.it/>.
- FEMA. [2007] *Interim Testing Protocols for Determining the Seismic Performance Characteristics of Structural and Nonstructural Components*, FEMA-461, Federal Emergency Management Agency, Washington, DC. pp. 138.

- FEMA. [2012] *Seismic Performance Assessment of Buildings: Volume 1 - Methodology (P-58-1)*, Federal Emergency Management Agency, Washington, DC.
- Filiatrault, A. and Christopoulos, C. [2002] “Guidelines, specifications, and seismic performance characterization of nonstructural building components and equipment,” *Report PEER 2002/05*, Pacific Earthquake Engineering Research Center, Berkeley, CA, pp. 102, doi:10.1044/1059-0889(2002/er01)
- Filiatrault, A. and Sullivan, T. [2014] “Performance-based seismic design of non-structural building components: the next frontier of earthquake engineering,” *Earthquake Engineering and Engineering Vibration* Special Issue on the State-of-the-art and Future Challenges of Earthquake Engineering **13**(1), 17–46. doi:10.1007/s11803-014-0238-9.
- Filiatrault, A., Tremblay, R., Christopoulos, C., Folz, B. and Pettinga, D. [2013] *Elements of Earthquake Engineering and Structural Dynamics*, Third ed., Polytechnic International Press, Montreal, Canada. pp. 874.
- Filiatrault, A., Uang, C. M., Folz, B., Christopoulos, C. and Gatto, K. [2001] “Reconnaissance report of the February 28, 2001 Nisqually (Seattle-Olympia) earthquake,” *Structural Systems Research Project Report No. SSRP-2000/15*, Department of Structural Engineering, University of California, San Diego, La Jolla, CA, pp. 62.
- Gupta, A. and McDonald, B. M. [2008] “Performance of building structures during the October 15, 2006 Hawaii earthquake,” *Proc. of the 14th World Conference on Earthquake Engineering*, Beijing, China, pp. 8.
- Hilti. [2014] *Earthquake Resistant Design of Installations*, 1.1 ed., Hilti Corporation, Schaan, Liechtenstein. pp. 104.
- Jacobsen, L. S. [1930] “Steady forced vibrations as influenced by damping,” *ASME Transactions American Society of Mechanical Engineers* **52**(1), 169–181.
- Jacobsen, L. S. [1960] “Damping in composite structures.” *Proc. of the 2nd World Conference in Earthquake Engineering, Vol. 2*, Tokyo and Kyoto, Japan, pp. 1029–1044.
- Jayaram, N., Lin, T. and Baker, J. W. [2011] “A computationally efficient ground-motion selection algorithm for matching a target response spectrum mean and variance,” *Earthquake Spectra* **27**(3), 797–815. doi:10.1193/1.3608002.
- Kehoe, B. and Hachem, M. [2003] “Procedures for estimating floor accelerations,” *Proc. Of the Seminar on Seismic Design, Performance, and Retrofit of Nonstructural Components in Critical Facilities, ATC 29–2*, Newport Beach, CA, pp. 361–374.
- Mazzoni, S., McKenna, F., Scott, M. H. and Fenves, G. L. [2006] *OpenSees Command Language Manual*, Pacific Earthquake Engineering Research Center, Berkeley, California.
- Meisel, P. W. [2001] “Static modeling of equipment acted on by seismic forces,” *ASHRAE Transactions* **107**(1), 775–786.
- Miranda, E. and Taghavi, S. [2003] “Estimation of seismic demands on acceleration-sensitive non-structural components in critical Facilities,” *Proc. of the Seminar on Seismic Design, Performance, and Retrofit of Non-structural Components in Critical Facilities, ATC 29–2*, Newport Beach, California, pp. 347–360.
- NRC. [2015] *National Building Code of Canada*, National Research Council, Ottawa, Canada. pp. 708.
- PEER [2018] NGA-West database, Pacific Earthquake Engineering Research Center, Berkeley, California, available on-line: <http://peer.berkeley.edu/ngawest>.
- Pekcan, G., Itani, A. and Staehlin, W. [2003] “Nonstructural system response to vertical excitation and implications for seismic design and qualification,” *Proc. of the Seminar on Seismic Design, Performance, and Retrofit of Nonstructural Components in Critical Facilities, ATC 29–2*, Newport Beach, California, pp. 387–398.
- Perrone, D., Calvi, P. M., Nascimbene, R., Fischer, E. and Magliulo, G. [2018] “Seismic performance and damage observation of non-structural elements during the 2016 Central Italy Earthquake,” *Bulletin of Earthquake Engineering* Accepted for Publication. doi:10.1007/s10518-018-0361-5.
- Priestley, M. J. N. [1993] “Myths and fallacies in earthquake engineering - conflicts between design and reality,” *Bulletin of the New Zealand National Society for Earthquake Engineering* **26**(3), 329–341.

- Priestley, M. J. N. [1998] "Displacement-based approaches to rational limit states design of new structures," *Proc. of the 11th European Conference on Earthquake Engineering*, Paris.
- Priestley, M. J. N. [2000] "Performance based seismic design," *Proc. of the 12th World Conference on Earthquake Engineering, Paper No. 2831*, Auckland, New Zealand.
- Priestley, M. J. N., Calvi, G. M. and Kowalsky, M. J. [2007] *Displacement-Based Seismic Design of Structures*, IUSS Press, Istituto Universitario di Studi Superiori di Pavia, Pavia, Italy. pp. 721.
- Ricci, P., De Luca, F. and Verderame, G. M. [2011] "6th April 2009 L'Aquila earthquake, Italy: reinforced concrete building performance," *Bulletin of Earthquake Engineering* **9**(1), 285–305. doi:10.1007/s10518-010-9204-8.
- Rozman, M. and Fajfar, P. [2009] "Seismic response of RC frame building designed according to old and modern practices," *Bulletin of Earthquake Engineering* **7**, 779–799. doi:10.1007/s10518-009-9119-4.
- Salvatore, W., Caprili, A. and Barberi, V. [2009] "Rapporto dei danni provocati dall'evento sismico del 6 Aprile sugli edifici scolastici del centro storico dell'Aquila," available online: <http://www.reluis.it/>.
- Singh, M. P., Moreschi, L. M., Suárez, L. E. and Matheu, E. E. [2006a] "Seismic design forces. I: rigid nonstructural Components," *Journal of Structural Engineering, American Society of Civil Engineering* **132**(10), 1524–1532.
- Singh, M. P., Moreschi, L. M., Suárez, L. E. and Matheu, E. E. [2006b] "Seismic design forces. II: flexible nonstructural Components," *Journal of Structural Engineering, American Society of Civil Engineering* **132**(10), 1533–1542.
- Soong, T. T. [1995] "Seismic behavior of nonstructural elements-state-of-the-art-report," *Proc. of the 10th European Conference on Earthquake Engineering*, Vienna, Austria, pp. 1599–1606.
- Sullivan, T. J., Calvi, P. M. and Nascimbene, R. [2013] "Towards improved floor spectra estimates for seismic design," *Earthquakes and Structures, an International Journal Techno Press* **4**(1), 109–132. doi:10.12989/eas.2013.4.1.109.
- Sullivan, T. J., Priestley, M. J. N. and Calvi, G. M. [2008] "Estimating the higher mode response of ductile structures," *Journal of Earthquake Engineering* **12**(3), 456–472. doi:10.1080/13632460701512399.
- Takeda, T., Sozen, M. A. and Nielsen, N. N. [1970] "Reinforced concrete response to simulated earthquakes," *Journal of the Structural Division American Society of Civil Engineering* **96**(12), 2557–2573.
- Tauby, J. R., Lloyd, R., Nice, T. and Tünnissen, J. [1999] *A Practical Guide to Seismic Restraint*, American Society of Heating, Refrigerating, and Air-Conditioning Engineers, Inc., Atlanta, GA.
- UBC. [1964] *Uniform Building Code*, 6th ed., International Conference of Building Officials, Whittier Narrow, California.
- Vukobratović, V. and Fajfar, P. [2016] "A method for the direct estimation of floor acceleration spectra for elastic and inelastic MDOF structures," *Earthquake Engineering & Structural Dynamics* **45**, 2495–2511. doi:10.1002/eqe.2779.
- Vukobratović, V. and Fajfar, P. [2017] "Code-oriented floor acceleration spectra for building structures," *Bulletin of Earthquake Engineering* **15**, 3013–3026. doi:10.1007/s10518-016-0076-4.
- Wood, R. L., Hutchinson, T. C., Hoehler, M. S. and Kreidl, B. [2014] "Experimental characterization of trapeze assemblies supporting suspended non-structural systems," *Proc. of the Tenth U.S. National Conference on Earthquake Engineering, Paper No. 905*, Anchorage, Alaska, pp. 10.